King Saud University

Arabian Journal of Chemistry

www.ksu.edu.sa
www.sciencedirect.com

ORIGINAL ARTICLE

Fluoride adsorption enhancement of Calcined-Kaolin/Hydroxyapatite composite

Teerawat Laonapakul [a,*], Tanaratchanon Suthi [a], Yuichi Otsuka [b], Yoshiharu Mutoh [c], Patamaporn Chaikool [d], Prinya Chindaprasirt [e,f]

[a] Department of Industrial Engineering, Faculty of Engineering, Khon Kaen University, Khon Kaen 40002, Thailand
[b] Department of System Safety, Nagaoka University of Technology, Nagaoka, Niigata 940-2188, Japan
[c] Professor Emeritus Nagaoka University of Technology, Nagaoka, Niigata 940-2188, Japan
[d] Department of Mechanical Engineering, Faculty of Engineering, Rajamangala University of Technology Isan Khon Kaen Campus, Khon Kaen 40000, Thailand
[e] Sustainable Infrastructure Research and Development Center, Department of Civil Engineering, Faculty of Engineering, Khon Kaen University, Khon Kaen 40002, Thailand
[f] Academy of Science, Royal Society of Thailand, Dusit, Bangkok 10300, Thailand

Abstract The use of waste or natural resources is an interesting approach to preparing adsorbent materials. Most adsorption materials are powder-based, making them impractical for a variety of applications. In this work, the natural kaolin clay and hydroxyapatite synthesized from biogenic waste were studied as defluoridation materials. The point of zero charge (pH_{PZC}), the fluoride adsorption capability and the adsorption isotherm of calcined kaolin and mixed calcined kaolin/hydroxyapatite in both powdered and moulded forms were investigated. The hardness of the moulded (post-formed) samples was tested before and after in immersion in a fluoride solution. The maximum hardness was 15.8 kilo-pounds for the post-formed calcined kaolin sample. Sample hardness values slightly decreased after immersion in a fluoride solution due to the formation of micro-cracks. Most samples presented high pH_{PZC} values, implying that these materials are suitable for the capture of fluoride anions. The adsorption properties varied with the ratio of calcined kaolin to hydroxyapatite. These properties for post-formed samples were different from those in powdered form. Post-formed samples showed higher fluoride adsorption. The maximum fluoride adsorption capacity and efficiency of the post-formed samples (calcined kaolin) at pH 3 were 1.74 F$^-$ mg/g and 87%, respectively. The sorption of fluoride of hydroxyapatite and mixed calcined kaolin/hydroxya-

* Corresponding author.
E-mail address: teerla@kku.ac.th (T. Laonapakul).
Peer review under responsibility of King Saud University.

ELSEVIER | **Production and hosting by Elsevier**

patite powders was found to have the form of the Langmuir isotherm, which indicates a monolayer adsorption on the adsorbent surface. Isotherms of calcined kaolin powder, post-formed calcined kaolin and mixed calcined kaolin/hydroxyapatite samples followed the Freundlich isotherm, which indicates multilayer adsorption on a heterogenous adsorbent surface.

1. Introduction

Waste and waste materials are becoming more of a concern in every country. The worldwide environment has suffered as a result of these wastes. Due to an increase about 1 % in meat consumption (327 million tons in 2018), large amounts of over 100 million tons a year of animal bone waste have been produced (Du et al., 2020). Like most biological waste, animal bone waste is usually disposed of through landfill and incineration with serious consequences for air pollution and global climate change (Amiri et al., 2021). To avoid serious consequences, promoting the efficient use of natural or waste materials is a major challenge for our planet. Nowadays, several natural or waste materials have been used to develop a variety of valuable products, including adsorbent materials for water treatment. In this research, the natural kaolin clay and hydroxyapatite synthesized from biogenic waste (bovine bone) were studied as adsorbent materials for water defluoridation. This not only use natural resources, but economic and environmental benefits are obtained through waste recovery. Fluoride (F^-) is a occurring naturally inorganic mineral that is found at various concentrations in water, soil, and foods. High fluoride concentrations in surface or ground water and the risk from fluoride associated with using such water for human consumption are problems faced by people in developing countries. The consumption of water containing a small amount of fluoride has benefits for the human body, such as help preventing tooth decay. Long-term consumption of high concentrations of fluoride in drinking water can lead to health problems, including dental fluorosis, skeletal fluorosis, deformation of bones, and even lesions of organs (Xiong et al., 2007; Singh et al., 2016). Several techniques of fluoride removal, such as adsorption (He et al., 2020; Zhao et al., 2021), ion exchange (Swain et al. 2010), electrocoagulation (Oulebsir et al., 2020), chemical precipitation (Huang et al., 2017), membrane processes (Tahaikt et al., 2008) and reverse osmosis (Bejaoui et al., 2014) have been reported.

Adsorption is widely used in water and wastewater treatment processes due to its convenience, ease of operation and simplicity of design. It is a highly efficient technology that is economically viable (Bhatnagar et al., 2011; Loganathan et al., 2013). Various types of adsorbent materials, including hydroxyapatite (Mourabet et al., 2015; Wang et al., 2011), bone char (Leyva-Ramos et al., 2010), kaolinite (Nabbou et al., 2019; Meenakshi et al., 2008), clay (Uddin et al., 2019), fly ash (Xu et al., 2011), bentonite (Zhang et al., 2013), activated carbon (Pongener et al., 2018) and fluorspar and quartz (Fan et al., 2003) have been studied for use as materials for defluorination. The point of zero charge, pH_{PZC}, is the pH value at which the net surface charge of a material becomes equal to zero under given conditions (temperature, applied pressure, and aqueous solution composition) (Bakatula et al., 2018; Mahmood et al., 2011). Materials with low pH_{PZC} values are well suited to treatment of effluents contaminated with cations, while substrates with high pH_{PZC} are better suited to the capture of anions. Consideration of the point of zero charge could help to optimise the selection of materials and conditions for treatment of fluoride contaminated water.

Hydroxyapatite (HAp; $Ca_{10}(PO_4)_6(OH)_2$) is one of the most important calcium phosphates. HAp can be produced from biogenic wastes by various methods (Laonapakul, 2015; Laonapakul et al., 2021), including thermal decomposition (Sutthi et al., 2020). This method has many advantages, including its simple synthesis, favourable economic approach, use of biogenic wastes and the potential for mass production. Various powdered forms of HAp (including nano-HAp, glass-delivered HAp, and HAp synthesized from animal bones and shells) have attracted attention for their fluoride adsorption capabilities. Maximal fluoride adsorption occurs in the pH range of 5 to 7.3, with a variation of adsorption capacity depending on the properties and characteristics of the prepared HAp (Jimenez-Reys and Solache-Rios, 2010; Liang et al., 2011; Sundaram et al. 2009; Samant et al., 2017; Asgari et al., 2019). In the literature, only HAp in powdered form was used to study fluoride adsorption. Use of powdered HAp may be inconvenient for a variety of practical reasons. In the adsorption process, the adsorbents (such as chitosan and cerium oxide) often used in the form of flakes or powders could cause the high pressure drop, column blockage, and low flow rate. It affects the filtration during field applications and not suitable for the large-scale column operation (Habuda-Stanić et al., 2014; Lin et al., 2018). Calcined kaolin (CK) is one of the most important clay minerals containing SiO_2 and Al_2O_3 as its main components. CK can be produced by heating kaolin clay to high temperatures. The calcination process further increases its usability and creates an engineered product that increases whiteness, hardness and adjusts the size and shape of the kaolin particles. It is used as a starting material to obtain geopolymer composites with high strength. The mechanical properties of CK geopolymer are enhanced by hot curing (Davidovits and Davidovics, 2009; Pangdaeng et al., 2015; Hassaan et al., 2015; Rowles and O'connor, 2003). However, only the literature of kaolin clay (kaolinite) is available on fluoride adsorption. Nabbou et al. (2019) and Ayalew (2020) studied groundwater defluoridation using natural kaolin powder in an adsorption technique. Fluoride ion removal was efficient at pH values from 4 to 6, achieving maximum fluoride removals of 75 % to 90 %. Fluoride removal efficiency depends on a number of factors such as pH, particle size, adsorbent dose and contact time. To the best of our knowledge, there has been no attempt to produce a combined CK and HAp material to study fluoride ion adsorption. This study is thus directed towards the fabrication of a novel material for fluoride removal from water. The effect of forming on fluoride adsorption enhancement of CK/HAp was investigated to access the feasibility for practical application. The point of zero charge (pH_{PZC}), the fluoride adsorption capability and the adsorption isotherm of calcined kaolin and mixed calcined kaolin/hydroxyapatite in both powdered and moulded forms were investigated as they are the important parameters of fluoride adsorption materials. The mechanical property of moulded materials was also evaluated.

2. Materials and methods

2.1. Sample preparation and mechanical testing

The CK powder used in this study was prepared by calcination of kaolin clay at 600 °C in an electric furnace. Kaolin clay was obtained from the southern region (Ra-Nong province) of Thailand. The chemical composition of the resulting CK powder determined using an X-ray fluorescence (WDXRF, AXios mAX) is shown in Table 1. The HAp powder used in this study was prepared from bovine bones using a thermal decomposition method (Sutthi et al., 2020). This method produced a highly crystalline phase of HAp. CK and synthesised HAp

Table 1 Chemical composition of the CK powder.

Chemical composition	SiO_2	Al_2O_3	Ti_2O	Fe_2O	CaO	MgO	SO_3	LOI
wt (%)	58.68	36.71	1.43	1.06	0.25	0.07	0.03	1.77

were crushed into a powder and then sifted through a 100-mesh screen and stored in a desiccator. Sodium hydroxide (10 M, AGC Chemicals, Thailand), sodium silicate (15.32 % Na_2O, 32.87 % SiO_2, and 51.81 % H_2O, Eastern Silicate, Thailand) were used as liquid activated binders for the formation of mixed CK and HAp powders.

Sodium hydroxide and sodium silicate were prepared in a weight ratio of 1:1 to produce a liquid binder (alkali activator solution) (Pangdaeng et al., 2018). A 1:1 ratio of mixed powder to liquid binder was used to prepare the paste samples. CK/HAp powders with CK to HAp weight ratios of 1:0 (CK100), 3:1 (CK75), 1:1 (CK50), and 1:3 (CK25) were prepared by mixing the necessary materials in a planetary mixer for 5 min. An activated binder solution was then added and mixing was continued for another 5 min. The resulting fresh pastes were then poured into acyclic round tablet moulds (2 mm in thickness and 5 mm in diameter). They were vibrated for 15 s to remove entrapped air and wrapped in a cling film to prevent moisture loss. The samples were then cured in an electric oven at 60 °C for 14 days (Sutthi et al., 2018). The samples were demoulded (denoted as post-formed samples) and stored in a desiccator.

The post-formed samples were soaked in aqueous water with a 10 mg L^{-1} concentration of fluoride for 24 and 48 h to study the effect of fluoride adsorption on sample hardness. After soaking, the samples were taken out of the fluoride solution, gently washed with distilled water, dried at ambient temperature for 3 h, and then at 30 °C for one day in an incubator. The hardness tests were conducted using a Varian table hardness tester (Varian VK 200, Varian). The results were reported as averaged values of ten samples. The crystallinity of sample powders was investigated using X-ray Diffraction (XRD, Bruker D8) at a scan rate of 2.4° 2θ/min scanning in 0.02° 2θ increments with CuKα radiation. Morphological observations of the products were done using scanning electron microscopy (SEM, TESCAN MIRA, backscattered electron detector) at a 15 kV accelerating voltage.

2.2. Measurement of pH_{PZC}

The pH_{PZC} of both powders and post-formed samples were measured using a salt addition method to evaluate the appropriate pH conditions for fluoride sorption of materials. 0.1 M sodium chloride (NaCl) solutions at pH 2, 3, 4, 5, 6, 7, 8, 9, 10, 11, and 12 were prepared. The pH values of the NaCl solutions were adjusted with 0.1 M hydrochloric acid (HCl) or 0.1 M sodium hydroxide (NaOH), as appropriate. A mass of 0.1 g of mixed powders or post-formed samples was added to 50 mL of a 0.1 M NaCl solution in a 60 mL polyethylene (PE) bottle. The initial pH value in each tube was denoted as pH_i. The liquid samples were shaken for 48 h using a rotary agitator at 200 rpm and room temperature (25–28 °C). After

that, the liquid samples were left to settle for 1 h. The pH value of the supernatant in each bottle was then measured and denoted as pH_f. The pH_{PZC} of each sample was obtained from a plot of ΔpH ($= pH_f - pH_i$) against pH_i.

2.3. Fluoride adsorption

2.3.1. Effect of pH

A study of fluoride adsorption was conducted in batch-mode experiments to optimise initial pH values, which had some effect on the adsorption ability of materials. Batch-mode adsorption studies were carried out with 100 mL of a solution with an initial fluoride concentration of 10 mg/L in a 150 mL PE bottle. The effect of pH on the adsorption capacity and efficiency was investigated by adding 0.5 g of mixed powders or post-formed samples to the prepared fluoride solutions (pH of 2 to 12). A batch adsorption test was carried out for 48 h for each tested sample using a rotary agitator at 200 rpm. The pH value was re-adjusted to the initial values every 3 h. Calibration of the pH meter was done before every measurement using calibration buffers. All experiments were conducted at room temperature. The fluoride concentration was analysed with a wavelength scanning method using a spectrophotometer (Hach, DR 6000). The fluoride adsorption capacity, q_e (mg/g), of the adsorbent at equilibrium was calculated using the following equation (Gitari et al., 2020; Goswami and Purkait, 2014):

$$q_e = \frac{(C_0 - C_e) \times V}{m} \tag{1}$$

where C_0 and C_e are, respectively, the initial and equilibrium concentrations of the fluoride solution in mg/L, m is the mass of adsorbent in g, and V is the volume of fluoride solution in L.

The fluoride adsorption efficiency (percent fluoride adsorption) was calculated using the following equation (Gitari et al., 2020; Goswami and Purkait, 2014):

$$\text{percent fluoride adsorption} = \frac{C_0 - C_e}{C_0} \times 100 \tag{2}$$

2.3.2. Adsorption isotherms

Fluoride adsorption on mixed powders or post-formed samples was performed in batch-mode experiments. A 0.5 g mass of adsorbent was suspended in 100 mL of fluoride solutions of various concentrations (10–100 mg/L) in 150 mL PE bottles and shaken for 48 h at room temperature using a rotary agitator at 200 rpm. The pH values were re–adjusted to the initial values every 3 h. The most frequently used isotherms, Freundlich and Langmuir, were employed to model the experimental data of equilibrium adsorption isotherms for fluoride ions onto the mixed powders and post-formed samples. The Langmuir adsorption isotherm (Chung et al., 2015; Veloso

et al., 2020) is one of the best-known isotherms. It is often applied to liquid systems to describe saturated monolayer adsorption on an adsorbent surface. The equation for this isotherm is:

$$q_e = \frac{q_m K_L C_e}{1 + K_L C_e} \tag{3}$$

The linear form of the Langmuir adsorption isotherm is represented as:

$$\frac{C_e}{q_e} = \frac{1}{K_L q_m} + \frac{C_e}{q_m} \tag{4}$$

where q_e (mg/g) is the amount of fluoride adsorbed per unit mass of the adsorbent at equilibrium, q_m (mg/g) is the maximum amount of fluoride per unit weight of adsorbent to form a complete monolayer on the surface, K_L (L/mg) is an adsorption equilibrium constant, and C_e (mg/L) is the equilibrium concentration of fluoride in a solution. The defining characteristics of the Langmuir isotherm can be classified by the separation factor R_L (Ayawei et al., 2017) in the following equation:

$$R_L = \frac{1}{1 + K_L C_O} \tag{5}$$

where K_L is Langmuir constant (L/mg) and C_o is initial concentration of adsorbate (mg/L).

When:

(i) R_L greater than 1 there is an unfavorable adsorption process, encouraging a desorption.
(ii) R_L = 1 indicates a linear adsorption process (the adsorption is independent of concentration).
(iii) R_L = 0 is an irreversible adsorption process where the adsorbed adsorbate cannot diffuse or desorb. This commonly occurs in chemisorption.
(iv) $0 < R_L < 1$ indicates a favourable adsorption process, discouraging a desorption process.

The Freundlich adsorption isotherm (Chung et al., 2015; Veloso et al., 2020) describes multilayer adsorption with a non-uniform distribution on a heterogeneous surface. It is expressed as:

$$q_e = K_F C_e^{1/n} \tag{6}$$

In linear form, the Freundlich adsorption isotherm is:

$$\ln q_e = \ln K_F + \frac{1}{n} \ln C_e \tag{7}$$

where q_e (mg/g) is the equilibrium amount of fluoride adsorbed per unit mass of the adsorbent, C_e (mg/L) is the equilibrium concentration of fluoride in the bulk solution, K_F ($L^{1/n}$ $mg^{(1-1/n)}$/g) is a constant (Freundlich coefficient) indicative of adsorption capacity of the adsorbent, and the dimensionless constant $1/n$ indicates a function of the strength of adsorption in the process or surface heterogeneity. Its value ranges between zero and one. If $1/n$ is less than 1, this indicates a normal adsorption. Alternatively, when $1/n$ is greater than 1, cooperative adsorption is indicated where adsorbed adsorbate affects and influences the adsorption of free adsorbates (Tan et al., 2008).

3. Results and discussion

3.1. Post-formed and crystalline structure of adsorbent samples

The appearance of post-formed samples (CK100, CK75 and CK50) is shown in Fig. 1. A compact tablet shape is seen in post-formed samples. The formation of samples was unsuccessful when the proportion of CK was less than 50 % by weight. The XRD patterns of the substrate (CK and HAp) powders and mixed powders (CK75 and CK50) as well as the post-formed samples (CK100, CK75 and CK50) are depicted in Fig. 2 (a) and (b), respectively. Characteristic peaks of kaolinite and quartz were observed in CK powder. The high intensity characteristic peaks of hydroxyapatite were observed in HAp powder produced from bovine bones using a thermal decomposition method. The standard diffraction ICDD No. 00-001-0527 was referenced to kaolinite, ICDD No. 01-070-7345 to quartz and ICDD No. 09-0432 to HAp. Characteristic peaks of the substrate powders of CK co–existing with HAp were clearly observed in CK75 and CK50 mixed powders. The characteristic peak intensities of HAp increased with the HAp mixing ratio into CK. After formation, the characteristic peaks of the samples for each of the mixing ratios were not significant different between the mixed powders and post-formed samples. However, increases in the broad peaks on the XRD patterns were observed due to the geopolymerization reaction of substrates.

3.2. Effect of fluoride immersion on hardness of post-formed samples

The mean hardness values (in kilo-pounds, kp) of samples after post-forming and after immersion in a fluoride solution

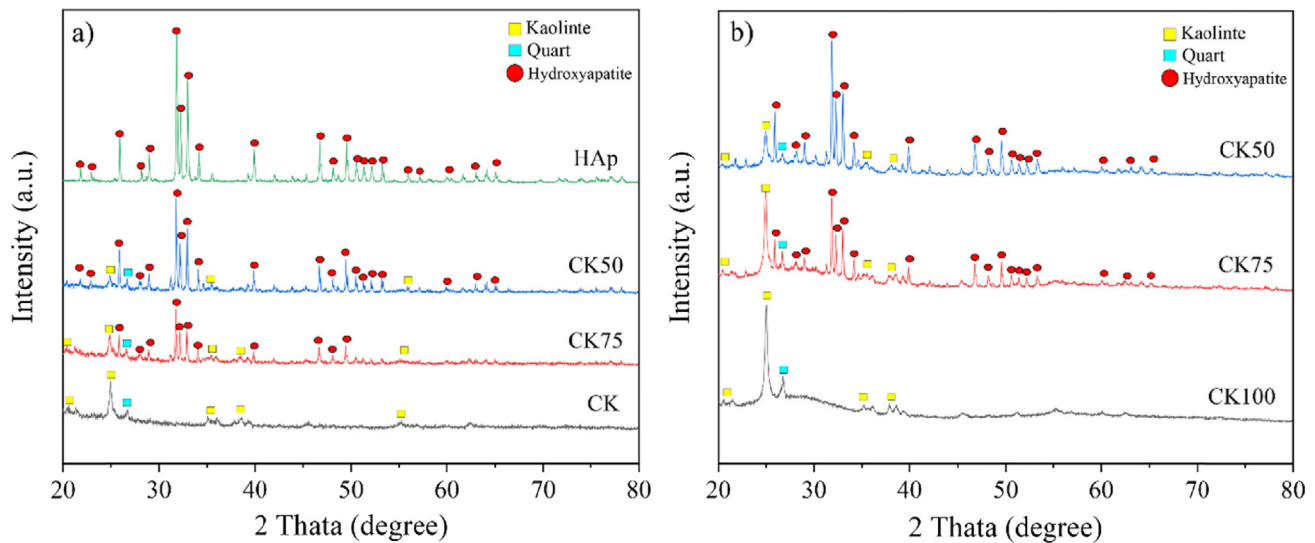**Fig. 1**   The post-formed samples of CK100, CK75 and CK50.

Fig. 2 The XRD patterns of (a) the substrate (CK and HAp) powders and the mixed powders and (b) the post-formed samples (CK100, CK75 and CK50).

at a concentration of 10 mg L^{-1} for 1 and 2 days are presented in Fig. 3. The hardness of post-formed samples decreased when HAp was mixed with CK. Maximal hardness of the post-formed sample without HAp (CK100) was 15.8 kp. The hardness of samples was less than 5 kp in samples containing 50 % HAp. It can be concluded that the formability and hardness of the samples was affected by the reaction of the CK geopolymer. The reaction was mainly between CK and the alkaline solution (sodium hydroxide and sodium silicate). A large amount of CK led to an improvement in sample strength due to the dissolution of silica and alumina species in the alkali activator solution, which subsequently promoted polycondensation phenomena and the formation of a geopolymeric binder. This results in the formation of an amorphous phase and a three-dimensional aluminosilicate network structure (Prud'Homme et al., 2011; Ren et al., 2017). Therefore, the unformable sample (the proportion of C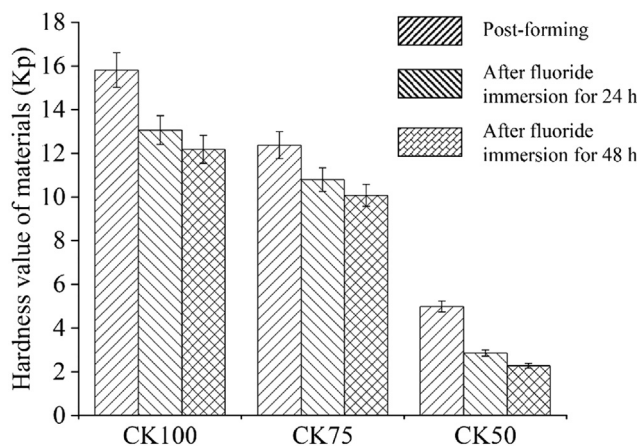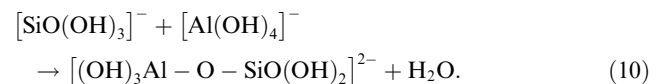K less than 50 % weight) results from the less amount of silica and alumina species in sample. This agrees with the results observed by Sutthi et al. (2016). The alkali activator solution has high capability to dissolve Si^{4+} and Al^{3+} ions from aluminosilicate materials in the CK. These ions are formed into aluminate and silicate tetrahedral monomers due to the alkali activator and then they polymerize as stable oligomers, according to the following reaction (Prasanphan et al., 2019):

$$Al_2O_3 + 3H_2O + 2OH^- \rightarrow 2\left[Al(OH)_4\right]^- \tag{8}$$

$$SiO_2 + H_2O + OH^- \rightarrow \left[SiO(OH)_3\right]^- \tag{9}$$

$$\left[SiO(OH)_3\right]^- + \left[Al(OH)_4\right]^-$$
$$\rightarrow \left[(OH)_3Al - O - SiO(OH)_2\right]^{2-} + H_2O. \tag{10}$$

After fluoride immersion, no degradation of the formed samples was observed on the basis of visual inspection. The hardness values of the CK100 and CK75 post-formed samples slightly decreased when the samples were immersed in a fluoride solution for periods of 24 and 48 h. The mean hardness decreased by 15 % compared to the post-formed samples for each mixing ratio. The decreased hardness was significant for the CK50 sample. There was no significant difference in the hardness of fluoride-immersed samples over 24 and 48 h for the CK100 and CK75 samples.

Observations of the surface morphology of the post-formed samples were done before and after immersion in a fluoride solution for periods of 24 and 48 h. Micro-cracks on the sample surfaces increased after fluoride immersion, as shown in Fig. 4, resulting in reduced hardness. This was due to the incomplete polymerization of mixed materials. Water or other liquids can be absorbed by geopolymers. Two types of water viz., free and bound water, are generally absorbed in geopolymers (Azwa et al., 2013). Free water molecules can flow freely through micro-voids or pores, while bound water molecules are associated with the polar groups of the geopolymer matrix (Alomayri et al., 2014). Therefore, the molecules of the fluoride solution could move independently through the micro-voids
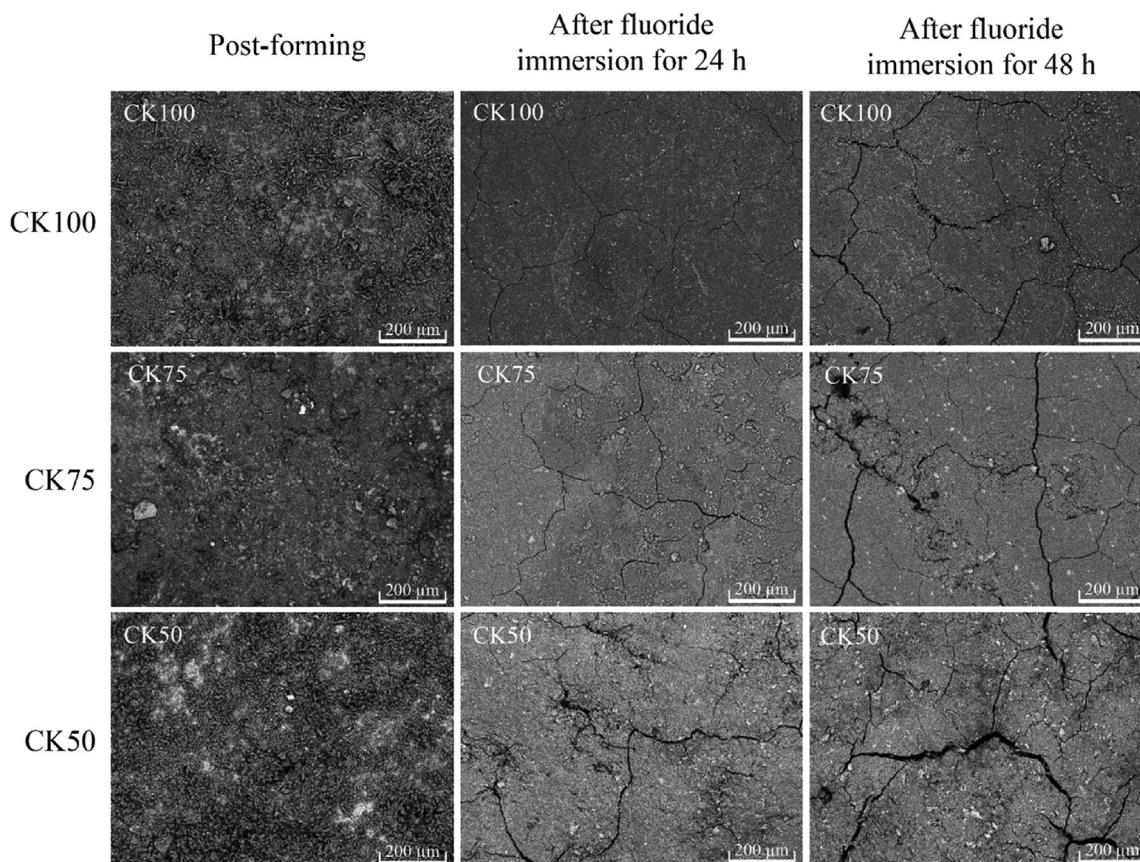

Fig. 3 The average hardness value of the samples after post-formed and after immersion in a fluoride solution at a concentration of 10 mg/L for 1 and 2 days.

Fig. 4 The surface morphology of the post-formed samples and after immersed in a fluoride solution for 24 and 48 h.

and pores of the post-formed samples. This also had the effect of removing unreacted alkaline solution and CK, resulting in the creation of micro-cracks on the surface and inside the formed sample.

3.3. Effect of HAp mixing and sample formation on pH_{PZC}

To clearly understand the effect of pH on the adsorption materials, the point of zero charge, pH_{PZC} values of the substrate powders (CK and HAp), the powders mixed various ratios, and the post-formed samples (CK75 and CK50) were investigated. The observed pH_{PZC} values of the CK and HAp powders were 6.1 and 10.5, respectively, as shown in Fig. 5 (a) and (b). Similar results were reported by Nabbou et al. (2019) and Hernández-Barreto et al. (2022) that the pH_{PZC} values of kaolin and HAp (from bone waste) were 6.4 and 9.7, respectively. Dimović et al. (2009) reported that the pH_{PZC} value of HAp varied between 6.83 and 10.15. It increased with the increasing heat-treating temperature of animal bone. The addition of HAp powder into CK powder resulted in a change of the pH_{PZC} value due to the disparate pH_{PZC} values of each powder. The pH_{PZC} values of the CK75 and CK50 powders were 9.3 and 9.75, respectively, as shown in Fig. 6 (a) and (b).

Fig. 7 shows the observed pH_{PZC} values of the samples (CK100, CK75, and CK50) that were formed by geopolymerisation. pH_{PZC} values of the CK100, CK75, and CK50 samples were 9.9, 10.5, and 10.9, respectively. The pH_{PZC} of samples for all mixing ratios slightly increased after their formation.

This phenomenon resulted from a geopolymerization reaction between the mixed powder and binder, which changed the properties of materials. A high pH_{PZC} value implied that it would be suitable to capture the fluoride anions at pH values less than the pH_{PZC}.

3.4. Effect of pH on fluoride adsorption

The fluoride adsorption capacity and efficiency (according to Eqns. (1) and (2)) of materials in powdered form and post–formed samples in various proportions were studied at various pH values from 2 to 12 (Figs. 8–10). Fig. 8 (a) and (b) show the fluoride adsorption capacity and efficiency of CK and HAp powders. In CK powder, fluoride was adsorbed at pH 2 to 7. The maximum fluoride adsorption capacity of 1.75 F^- mg/g and efficiency of 87.5 %, were observed at pH 3. The fluoride adsorption capacity and efficiency decreased with increasing pH of the fluoride solution. HAp powder adsorbed fluoride at pH 5 to 10, with a maximum fluoride adsorption of 1.4 F^- mg/g and efficiency of 65 % at pH 6. When the pH in fluoride solution was greater than 6, the efficiency of absorption decreased. The fluoride adsorption capability changed when HAp powder was mixed with CK powder. The pH range for fluoride removal of mixed CK/HAp powders was between the pH ranges for fluoride removal of pure CK and HAp powders (Fig. 9). The fluoride adsorption capacity of CK/HAp powder decreased with increasing levels of HAp powder. The different of pH range on the fluoride adsorption between CK and HAp powders
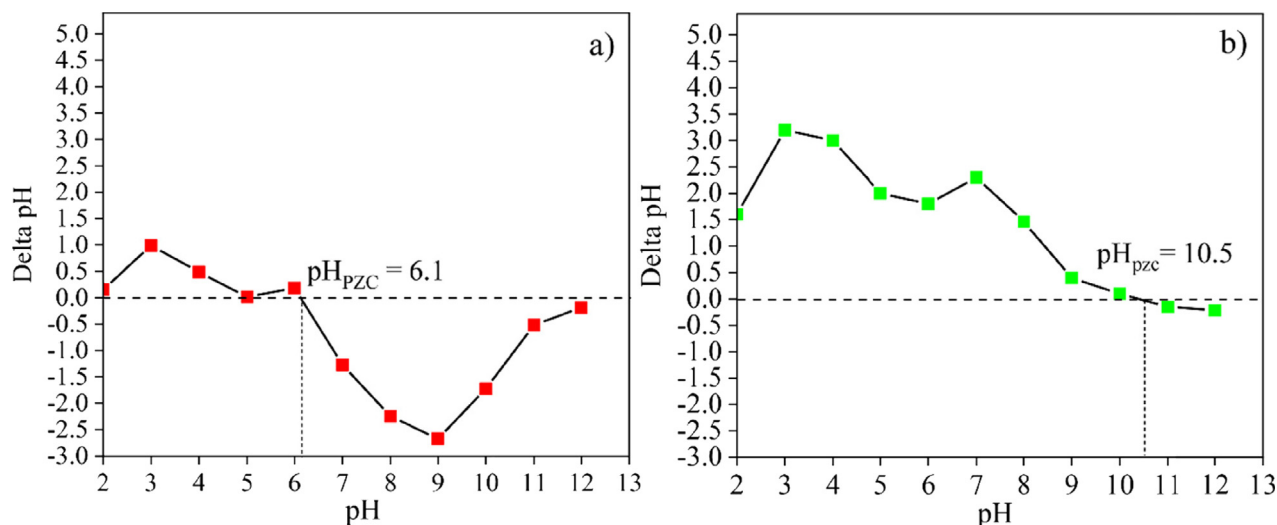
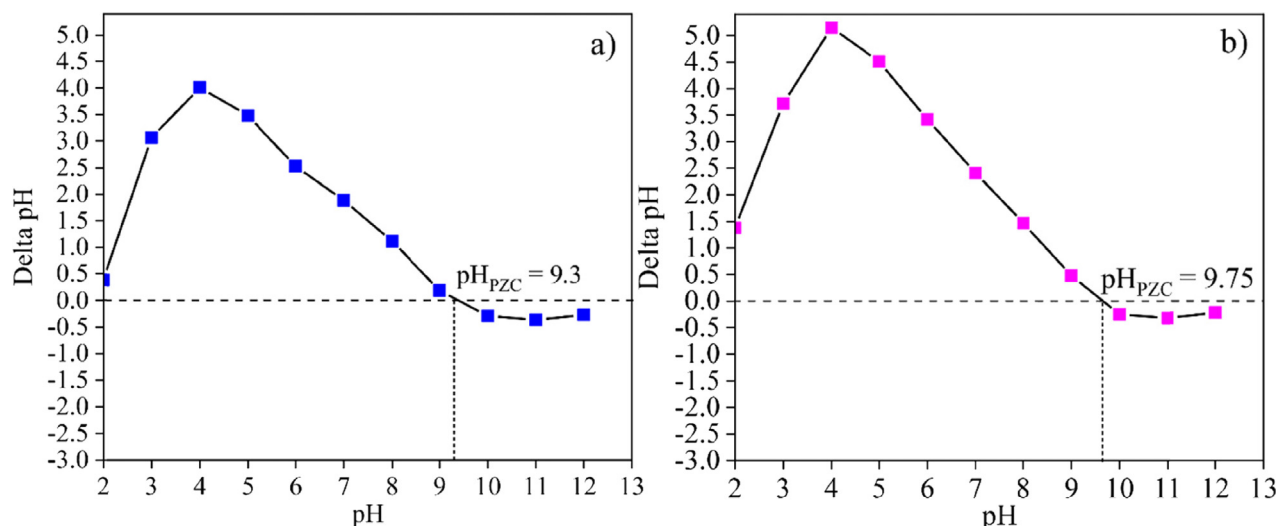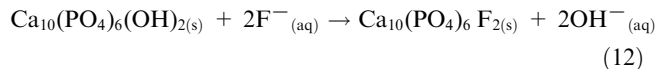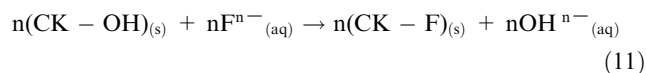**Fig. 5** The pH_{PZC} of (a) the calcined kaolin and (b) hydroxyapatite powders.

Fig. 6 The pH_{PZC} of (a) the CK75 and (b) CK50 powders.

probably decreased the adsorption capability of mixed CK/HAp powders. The results of the pH range on the fluoride adsorption of CK and HAp powders are in good agreement with the reports in the literatures (Nabbou et al., 2019; Jimenez-Reys and Solache-Rios, 2010). Mixed powders had the capability of adsorbing fluoride at pH 3 to 7. Maximal fluoride adsorption of CK75 powder was 1.05 F^- mg/g at pH 4, while that of the CK50 powder was 0.94 F^- mg/g at pH 5, as shown in Fig. 9 (a) and (b) with the corresponding maximum fluoride adsorption efficiencies of 52.7 % and 46.8 %, respectively. The samples powders could absorb fluoride at pH lower than that of pH_{PZC} of each sample. The fluoride adsorption at this level was due to the electrostatic interaction between the positive charged absorbent surface and negative charged fluoride ion. The chemical adsorption of fluoride could be explained by the following reactions (Kau et al., 1997; Sawangjang et al., 2021; Sani et al., 2016; Zúñiga-Muro et al., 2017):

$$n(CK - OH)_{(s)} + nF^{n-}_{(aq)} \rightarrow n(CK - F)_{(s)} + nOH^{n-}_{(aq)}$$
(11)

$$Ca_{10}(PO_4)_6(OH)_{2(s)} + 2F^-_{(aq)} \rightarrow Ca_{10}(PO_4)_6 F_{2(s)} + 2OH^-_{(aq)}$$
(12)

The samples remove fluoride from aqueous solution through an ion exchange mechanism between hydroxyl ($-OH$) groups and fluoride ions.

Fig. 10 shows the fluoride adsorption capacity and efficiency of post-formed materials. Post-formed CK100 adsorbed fluoride at pH 2 to 7. The fluoride adsorption capability of CK100 did not change after formation compared to the powder form. The maximum fluoride adsorption capacity and efficiency of the post-formed CK100 were 1.74 F^- mg/g and 87 %, respectively, at pH 3. Post-formed CK75 and CK50 adsorbed fluoride at pH 3 to 7. Maximal fluoride adsorption capability of post-formed CK75 and CK50 was improved compared to the same materials in powdered form. The maximum fluoride adsorption for CK75 and CK50 at pH 3 were 1.54 and 1.36 F^- mg/g, respectively. Maximal fluoride adsorption efficiencies of the post-formed CK75 and CK50 were 77 % and
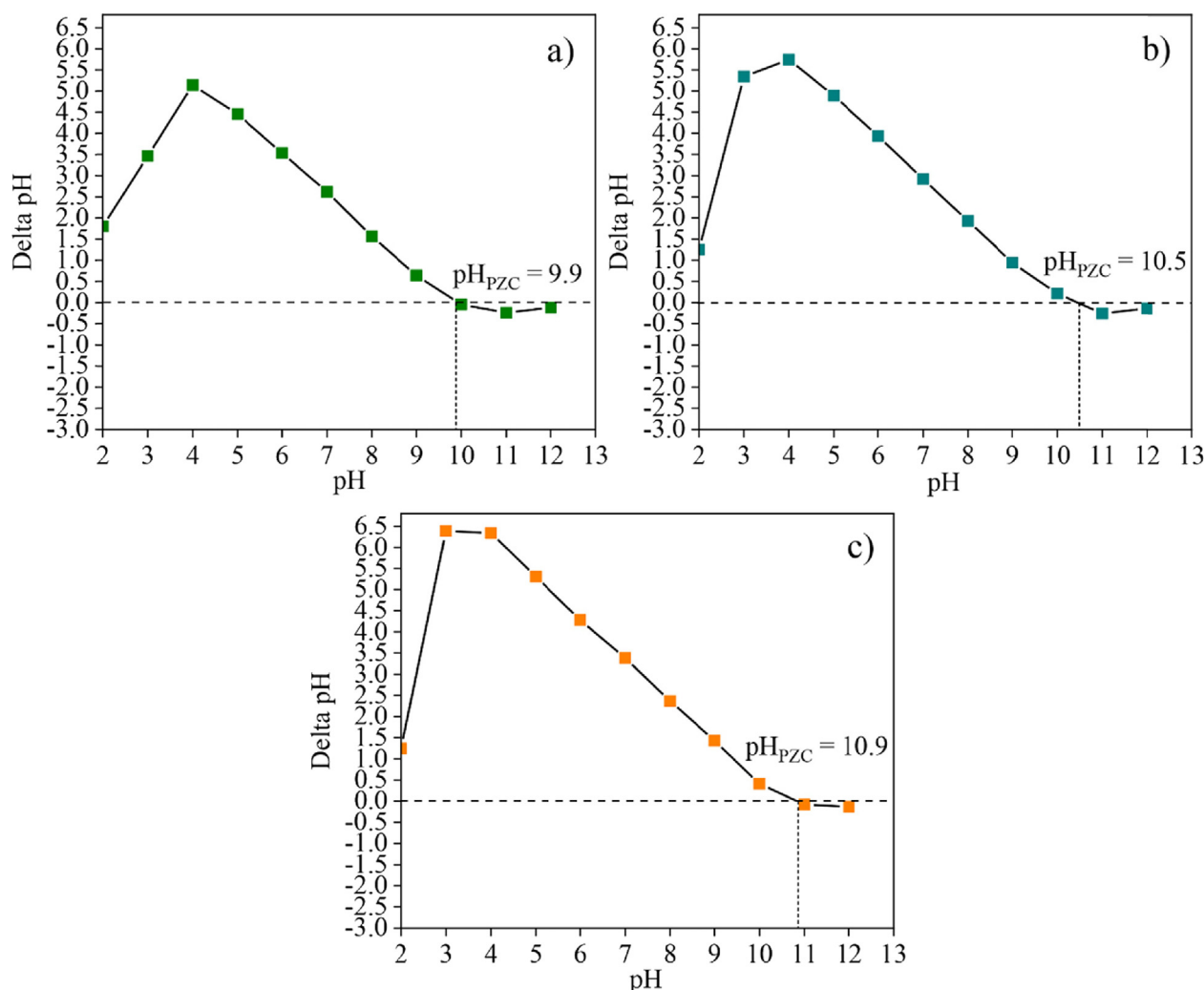
Fig. 7 The pH$_{PZC}$ of (a) post-formed CK100, (b) CK75 and (c) CK50 samples.

67.8 %, respectively. The enhancement in fluoride adsorption of the post-formed samples over powder samples was due to the increasing of –OH group in post-formed samples after geopolymerization as presented in Eqns. (8)–(10). The increasing of –OH group may provide additional adsorption sites resulting in high adsorption fluoride uptake. Their fluoride adsorption capacity and efficiency decreased with increasing pH of the fluoride solutions. This effect confirms earlier findings by Ayalew (2020), Sundaram et al. (2009) and Liang et al. (2011) that the adsorption of ions on kaolin and hydroxyapatite minerals declines as the pH of solution increases. Increasing the pH value leads to an increase in the number of negatively charged sites (hydroxyl ion, OH) on the adsorbents resulting in a decrease of the percent fluoride adsorption. This is probably due to the competition for adsorption sites between fluoride and hydroxyl ions on the absorbent surface. Geopolymerization of mixed CK and HAp samples affected their fluoride adsorption capability. Extensive study of their adsorption isotherms is needed to clarify the adsorption behaviours of these adsorbents.

3.5. Fluoride adsorption isotherms

The adsorption isotherms of adsorbents were investigated to clarify their behaviour. Experimental equilibrium data for adsorption of fluoride ions onto mixed powders and post–formed samples were analyzed by two often–used isotherm models, Langmuir and Freundlich. Batch-mode experiments were conducted at the maximum fluoride adsorption pH values of each adsorbent. Maximal adsorption capacity (q_m) and the Langmuir constant, as well as the values of K_F and n, were determined from the intercept and slope of linear plots using Equations (4) and (7) employing the linear trend function of Excel. Linear adsorption isotherm plots of $1/C_e$ versus $1/q_e$ and ln C_e versus ln q_e are shown in Figs. 11 and 12. The best fitted isotherm equations to the experimental data were evaluated based on their coefficients of determination (R^2) and two error functions, the symmetrical mean absolute percentage error (SMAPE) and the Chi–square test (χ^2). The data are summarized in Table 2. Maximal adsorption capacity (q_m) and the Langmuir constant, as well as the values of K_F and n calculated from the linear plot data were used to plot non-
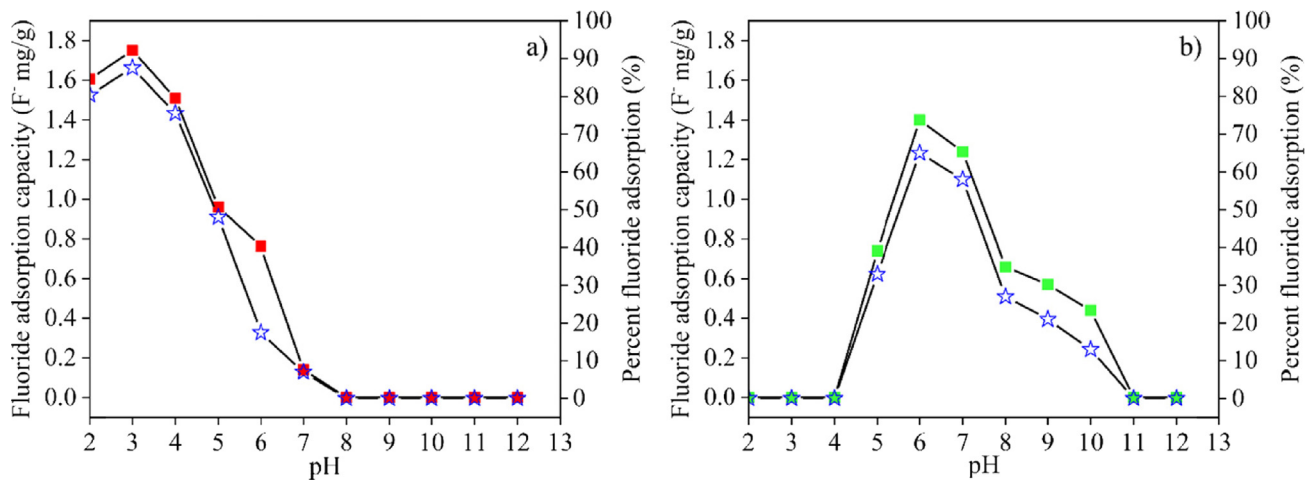
Fig. 8 The fluoride adsorption capacity (■) and efficiency (I) of (a) calcined kaolin and (b) hydroxyapatite powders.
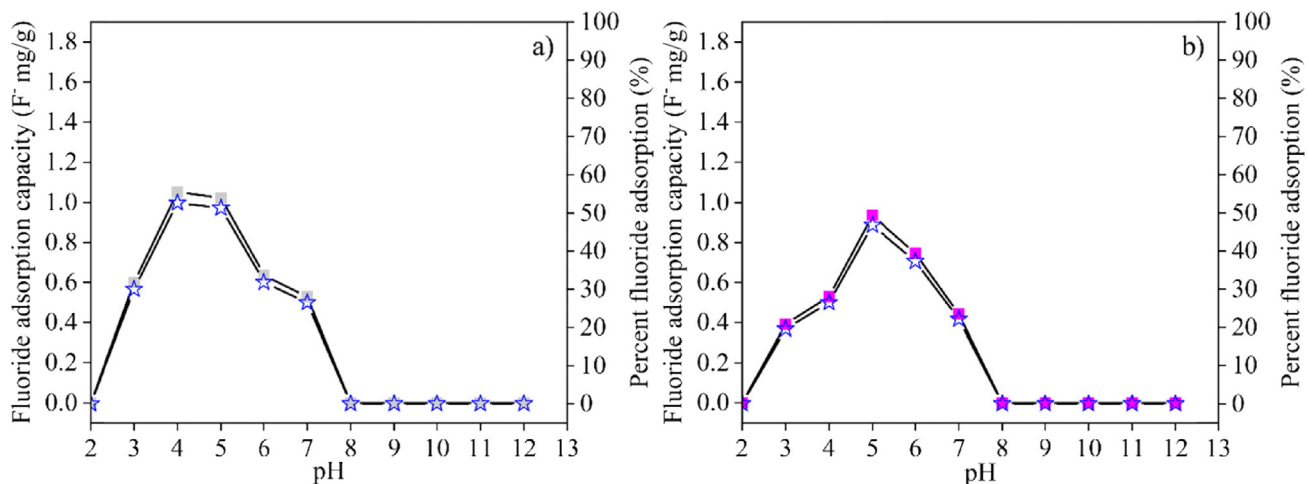

Fig. 9 The fluoride adsorption capacity (■) and efficiency (I) of (a) CK75 and (b) CK50 powders.

linear Langmuir and Freundlich isotherm using Equations (3) and (6). Plots of non-linear isotherm models and experimental equilibrium data are shown in Figs. 13 and 14.

The model with the best fit to experimental data was consider that with a higher coefficient of determination (R^2). The symmetrical mean absolute percentage error (SMAPE) and Chi–square tests (χ^2) were also considered in the case of small differences (less than0.01) in the values of R^2. According to the results of the isotherm study, higher R^2 values were obtained for the Langmuir isotherm model on HAp powder, and CK75 and CK50 mixed powder samples. The calculated value of R_L from Equation (5) was within the range of 0–1, thus confirming a favourable adsorption process for fluoride by HAp powder, as well as for CK75 and CK50 mixed powder samples. Higher R^2 and lower SMAPE or χ^2 values were obtained for the Freundlich isotherm on CK powder, CK100, CK75 and CK50 post-formed samples. Values of 1/n for these samples were less than 1 indicating a

normal adsorption process. Therefore, it can be concluded that the Langmuir isotherm describes monolayer adsorption of fluoride with a favourable adsorption process onto HAp powder, as well as CK75 and CK50 mixed powder samples. However, the Freundlich isotherm better describes multilayer adsorption of fluoride with a normal adsorption process onto CK powder, CK100, CK75 and CK50 post-formed samples.

Based on the results obtained from this study, it can be observed that the post-formed samples (CK100, CK75 and CK50) exhibited good performance with high strength for fluoride removal over a wide pH range. However, the batch adsorption study may not be applicable to the industrial scale. The extensive studies on the adsorption kinetics, the regeneration of fluoride ion and the column performance on the post-formed samples are required because they are effective in proving the practical applicability of the adsorbents for water treatment.
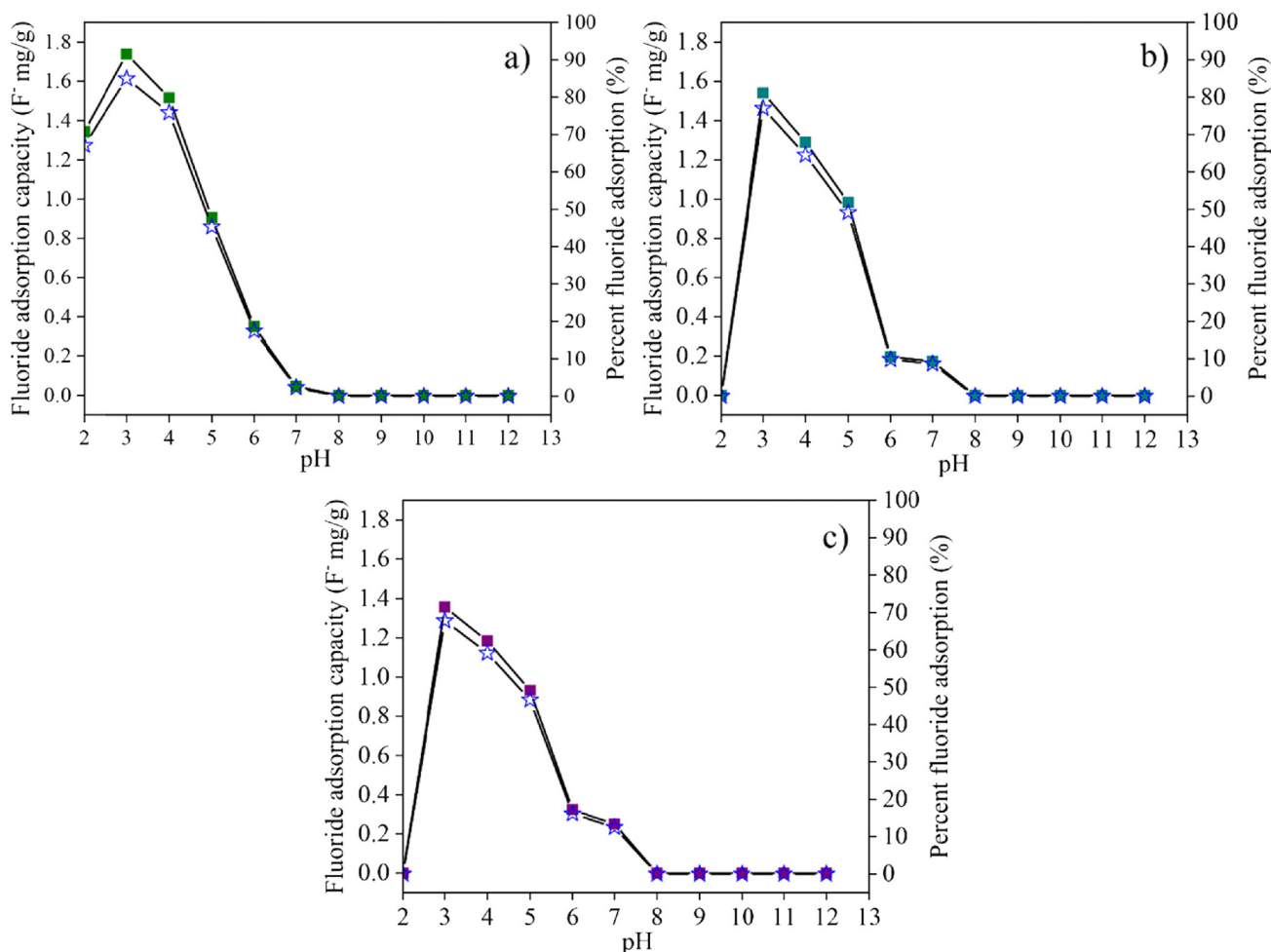
Fig. 10   The fluoride adsorption capacity (■) and efficiency (I) of (a) post-formed CK100, (b) CK75 and (c) CK50 samples.
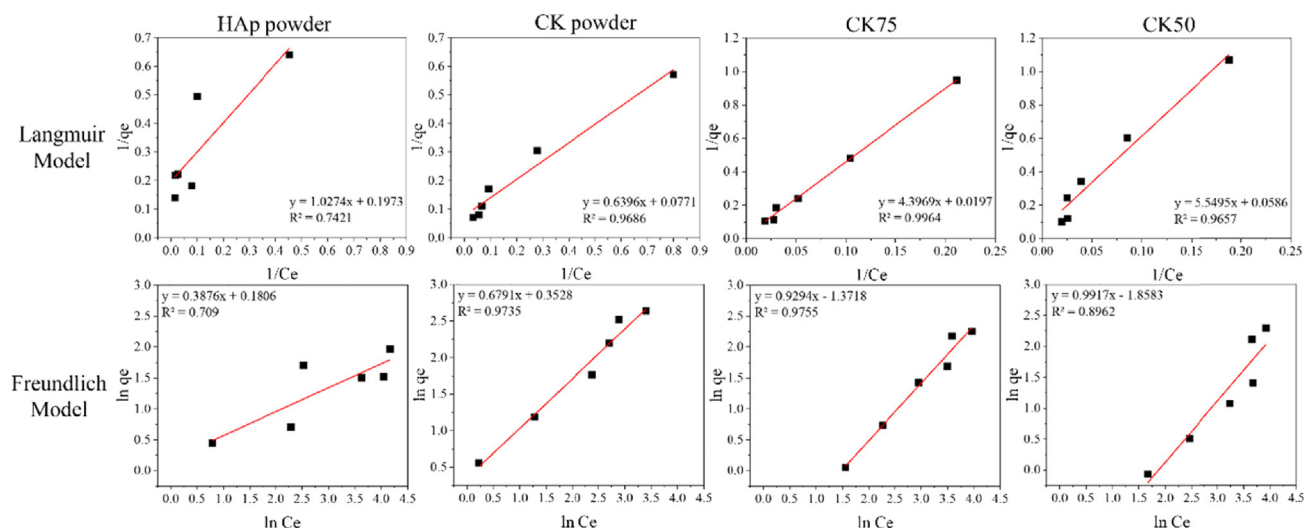

Fig. 11   Linear adsorption isotherm models of Langmuir and Freundlich for adsorption of mixed powder samples.
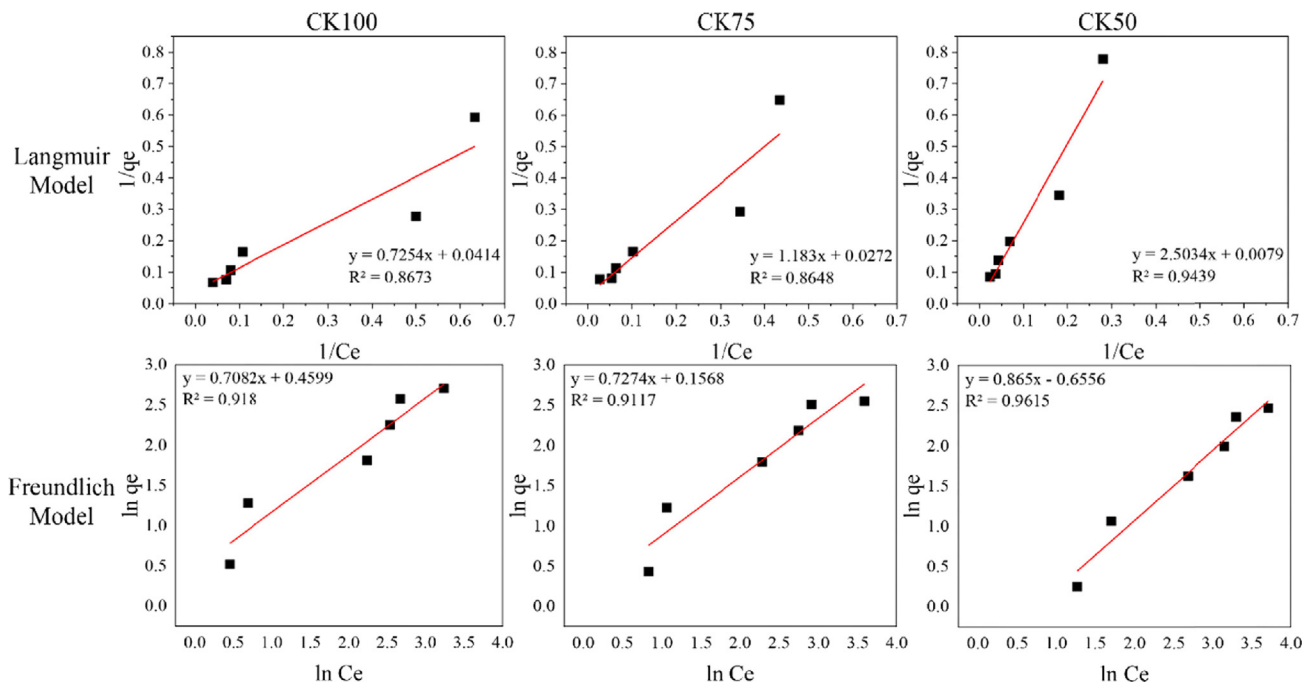
Fig. 12 Linear adsorption isotherm models of Langmuir and Freundlich for adsorption of post-formed samples.

Table 2 The adsorption isotherm parameters for adsorption of mixed powder and post-formed samples.

| Adsorbent (Mixed powder)	pH	Langmuir Model					Freundlich Model				
		q_m (mg/g)	K_L	R^2	Error function		K_F	n	R^2	Error function	
					SMAPE	χ^2				SMAPE	χ^2
CK	3	12.97	0.120	0.969	19.327	0.036	1.423	1.472	0.974	5.617	0.046
HAp	6	5.07	0.192	0.742	23.032	0.184	1.198	2.580	0.709	19.366	0.434
CK75	4	50.76	0.004	0.996	7.830	0.013	0.254	1.076	0.976	9.898	0.052
CK50	5	17.06	0.011	0.966	26.183	0.095	0.156	1.008	0.896	31.840	0.158
Adsorbent (Post-forming)	pH	Langmuir Model					Freundlich Model				
		q_m (mg/g)	K_L	R^2	Error function		K_F	n	R^2	Error function	
					SMAPE	χ^2				SMAPE	χ^2
CK100	3	24.15	0.057	0.867	19.130	0.077	1.584	1.412	0.918	15.554	0.252
CK75	3	36.76	0.023	0.865	19.265	0.078	1.170	1.375	0.912	17.214	0.280
CK50	3	126.58	0.003	0.944	15.164	0.046	0.519	1.156	0.962	16.386	0.176
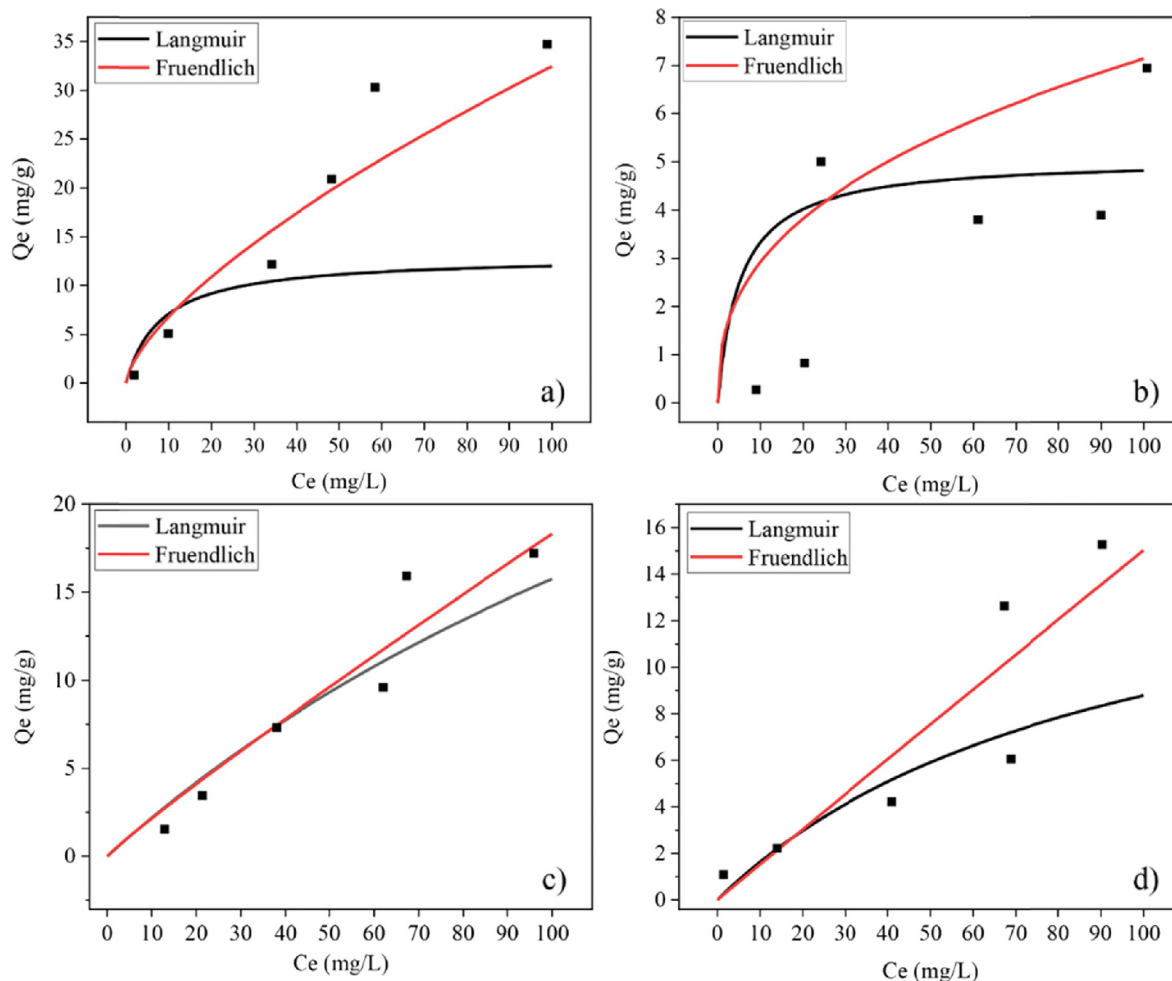
Fig. 13 Non-linier isotherm model plots for (a) CK (b) HAp (c) CK75 and (d) CK50 powders.

4. Conclusions

Tablet-shaped moulded samples of CK and CK/HAp were fabricated. The hardness of post–formed materials was evaluated. The pH_{PZC} and the effect of pH of the fluoride solution on the ability to adsorb fluoride by post-formed materials were studied and compared with the same materials in powdered form. The conclusions of this study are as follows.

(i) Formation of CK/HAp was successful when it was prepared with more than 50 wt% CK. The hardness of the post-formed samples was higher than 5 kp when they contained more than 50 wt% CK. The maximum hardness of post-formed samples was 15.8 kp for the CK100 sample. Hardness of the formed samples slightly decreased after immersion in fluoride solutions for 24 to 48 h.

(ii) The values of pH_{PZC} for the post-formed samples (CK100, CK75, CK50) and the powdered forms of CK75, CK50, and pure HAp were greater than 9, while the pH_{PZC} of CK powder was 6.1. The high value of pH_{PZC} indicates that these materials are suitable to capture fluoride anions at pH values lower than the pH_{PZC}.

(iii) The sorption of fluoride of HAp, CK75 and CK50 powders followed the Langmuir isotherm, indicating a monolayer adsorption on the adsorbent surface. Those of CK powder, post-

formed CK100 CK75 and CK50 followed the Freundlich isotherm, suggesting multilayer adsorption on a heterogenous adsorbent surface.

(iv) There was no significant difference between the fluoride adsorption capabilities of post–formed CK100 and CK powder. They were efficient at pH 2–6. Maximum fluoride adsorption capacity and percent fluoride adsorption of post-formed CK100 at pH 3 were 1.74 F^- mg/g and 87 %, respectively.

(v) The fluoride adsorption capability of CK/HAp (CK75 and CK50) improved after formation compared to the same ingredients in powder form. It was efficient pH 3–7. At pH 3, the maximum fluoride adsorption was 1.54 F^- mg/g for the post-formed CK75 and 1.36 F^- mg/g for the post-formed CK50 with respective efficiencies of 77 % and 67.8 %.

Declaration of Competing Interest
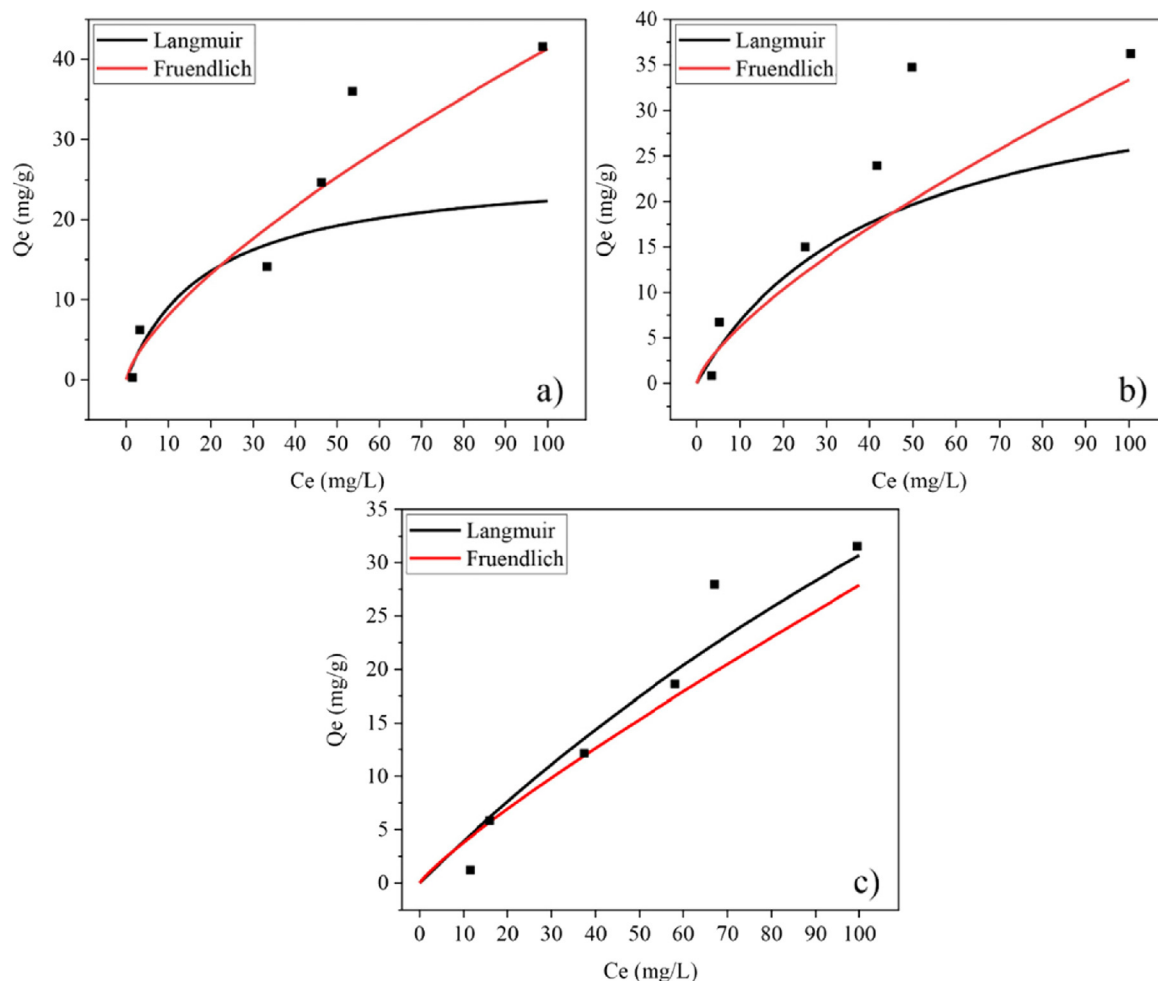
Fig. 14 Non-linier isotherm model plots for (a) CK100 (b) CK75 and (c) CK50 post-formed samples.

References

Alomayri, T., Assaedi, H., Shaikh, F.U.A., Low, I.M., 2014. Effect of water absorption on the mechanical properties of cotton fabric-reinforced geopolymer composites. J. Asian Ceram. Soc. 2 (3), 223–230. https://doi.org/10.1016/j.jascer.2014.05.005.

Amiri, M.J., Faraji, A., Azizi, M., Nejad, B.G., Arshadi, M., 2021. Recycling bone waste and cobalt-wastewater into a highly stable and efficient activator of peroxymonosulfate for dye and HEPES degradation. Process Saf. Environ. Prot. 147, 626–641. https://doi.org/10.1016/j.psep.2020.12.039.

Asgari, G., Dayari, A., Ghasemi, M., Seid-mohammadi, A., Gupta, V.K., Agarwal, S., 2019. Efficient fluoride removal by preparation, characterization of pyrolysis bone: Mixed level design experiment and Taguchi L$_8$ orthogonal array optimization. J. Mol. Liq. 275, 251–264. https://doi.org/10.1016/j.molliq.2018.10.137.

Ayalew, A.A., 2020. Development of Kaolin Clay as a Cost-Effective Technology for Defluoridation of Groundwater. Int. J. Chem. Eng. 2020, 8820727. https://doi.org/10.1155/2020/8820727.

Ayawei, N., Ebelegi, A.N., Wankasi, D., 2017. Modelling and interpretation of adsorption isotherms. J. Chem. 2017, 3039817. https://doi.org/10.1155/2017/3039817.

Azwa, Z.N., Yousif, B.F., Manalo, A.C., Karunasena, W., 2013. A review on the degradability of polymeric composites based on natural fibres. Mater. Des. 47, 424–442. https://doi.org/10.1016/j.matdes.2012.11.025.

Bakatula, E.N., Richard, D., Neculita, C.M., Zagury, G.J., 2018. Determination of point of zero charge of natural organic materials. Environ. Sci. Pollut. Res. 25, 7823–7833. https://doi.org/10.1007/s11356-017-1115-7.

Bejaoui, I., Mnif, A., Hamrouni, B., 2014. Performance of Reverse Osmosis and Nanofiltration in the Removal of Fluoride from Model Water and Metal Packaging Industrial Effluent. Sep. Sci. Technol. 49 (8), 1135–1145. https://doi.org/10.1080/01496395.2013.878956.

Bhatnagar, A., Kumar, E., Sillanpää, M., 2011. Fluoride removal from water by adsorption - A review. Chem. Eng. J. 171 (3), 811–840. https://doi.org/10.1016/j.cej.2011.05.028.

Chung, H.K., Kim, W.H., Park, J., Cho, J., Jeong, T.Y., Park, P.K., 2015. Application of Langmuir and Freundlich isotherms to predict adsorbate removal efficiency or required amount of adsorbent. J. Ind. Eng. Chem. 28, 241–246. https://doi.org/10.1016/j.jiec.2015.02.021.

Davidovits, J., Davidovics, M., 2009. Geopolymer: Room-temperature ceramic matrix for composites. In: Proceedings of the 12th Annual Conference on Composites and Advanced Ceramic Materials, Part

1 of 2: Ceramic Engineering and Science Proceedings, John Wiley & Sons, Inc. 2009. https://doi.org/10.1002/9780470310496.ch34.

Dimović, S., Smičiklas, I., Plećaš, I., Antonović, D., Mitrić, M., 2009. Comparative study of differently treated animal bones for Co^{2+} removal. J. Hazard. Mater. 164 (1), 279–287. https://doi.org/10.1016/j.jhazmat.2008.08.013.

Du, Q., Zhang, S., Antonietti, M., Yang, F., 2020. A sustainable leaching process of phosphates from animal bones to alleviate the world phosphate crisis. ACS Sustain. Chem. Eng. 8, 9775–9782. https://doi.org/10.1021/acssuschemeng.0c02233.

Fan, X., Parker, D.J., Smith, M.D., 2003. Adsorption kinetics of fluoride on low cost materials. Water Res. 37 (20), 4929–4937. https://doi.org/10.1016/j.watres.2003.08.014.

Gitari, W.M., Izuagie, A.A., Gumbo, J.R., 2020. Synthesis, characterization and batch assessment of groundwater fluoride removal capacity of trimetal Mg/Ce/Mn oxide-modified diatomaceous earth. Arab. J. Chem. 13 (1), 1–16. https://doi.org/10.1016/j.arabjc.2017.01.002.

Goswami, A., Purkait, M.K., 2014. Removal of fluoride from drinking water using nanomagnetite aggregated schwertmannite. J. Water Process Eng. 1, 91–100. https://doi.org/10.1016/j.jwpe.2014.03.009.

Habuda-Stanić, M., Ravančić, M.E., Flanagan, A., 2014. A Review on Adsorption of Fluoride from Aqueous Solution. Materials. 7, 6317–6366. https://doi.org/10.3390/ma7096317.

Hassaan, M.M., Khater, H.M., El-Mahllawy, M.S., El Nagar, A.M., 2015. Production of geopolymer composites enhanced by nano-kaolin material. J. Adv. Ceram. 4, 245–252. https://doi.org/10.1007/s40145-015-0156-y.

He, J., Yang, Y., Wu, Z., Xie, C., Zhang, K., Kong, L., Liu, J., 2020. Review of fluoride removal from water environment by adsorption. J. Environ. Chem. Eng. 8, (6). https://doi.org/10.1016/j.jece.2020.104516 104516.

Hernández-Barreto, D.F., Hernández-Cocoletzi, H., Moreno-Piraján, J.C., 2022. Biogenic Hydroxyapatite Obtained from Bone Wastes Using CO_2-Assisted Pyrolysis and Its Interaction with Glyphosate: A Computational and Experimental Study. ACS Omega. 7 (27), 23265–23275. https://doi.org/10.1021/acsomega.2c01379.

Huang, H., Liu, J., Zhang, P., Zhang, D., Gao, F., 2017. Investigation on the simultaneous removal of fluoride, ammonia nitrogen and phosphate from semiconductor wastewater using chemical precipitation. Chem. Eng. J. 307, 696–706. https://doi.org/10.1016/j.cej.2016.08.134.

Jimenez-Reys, M., Solache-Rios, M., 2010. Sorption behavior of fluoride ions from aqueous solution by hydroxyapatite. J. Hazard. Mater. 180 (1–3), 297–302. https://doi.org/10.1016/j.jhazmat.2010.04.030.

Kau, P.M.H., Smith, D.W., Binning, P., 1997. Fluoride retention by kaolin clay. J. Contam. Hydrol. 28 (3), 267–288. https://doi.org/10.1016/S0169-7722(96)00081-2.

Laonapakul, T., Sutthi, R., Chaikool, P., Talangkun, S., Boonma, A., Chindaprasirt, P., 2021. Calcium phosphate powders synthesized from $CaCO_3$ and CaO of natural origin using mechanical activation in different media combined with solid-state interaction. Mater. Sci. Eng. C. 118,. https://doi.org/10.1016/j.msec.2020.111333 111333.

Laonapakul, T., 2015. Synthesis of hydroxyapatite from biogenic wastes (review article). KKU Eng. 42 (3), 269–275 https://ph01.tci-thaijo.org/index.php/easr/article/view/38306.

Leyva-Ramos, R., Rivera-Utrilla, J., Medellin-Castillo, N.A., Sanchez-Polo, M., 2010. Kinetic modeling of fluoride adsorption from aqueous solution onto bone char. Chem. Eng. J. 158 (3), 458–467. https://doi.org/10.1016/j.cej.2010.01.019.

Liang, W., Zhan, L., Piao, L., Russel, C., 2011. Fluoride removal performance of glass derived hydroxyapatite. Mater. Res. Bull. 46 (2), 205–209. https://doi.org/10.1016/j.materresbull.2010.11.015.

Lin, J., Wu, Y., Khayambashi, A., Wang, X., Wei, Y., 2018. Preparation of a novel CeO_2/SiO_2 adsorbent and its adsorption

behavior for fluoride ion. Adsorpt. Sci. Technol. 36, 743–761. https://doi.org/10.1177/0263617417721588.

Loganathan, P., Vigneswaran, S., Kandasamy, J., Naidu, R., 2013. Defluoridation of drinking water using adsorption processes. J. Hazard. Mater. 248–249, 1–19. https://doi.org/10.1016/j.jhazmat.2012.12.043.

Mahmood, T., Saddique, M.T., Naeem, A., Westerhoff, P., Mustafa, S., Alum, A., 2011. Comparison of Different Methods for the Point of Zero Charge Determination of NiO. Ind. Eng. Chem. Res. 50 (17), 10017–10023. https://doi.org/10.1021/ie200271d.

Meenakshi, S., Sundaram, C.S., Sukumar, R., 2008. Enhanced fluoride sorption by mechanochemically activated kaolinites. J. Hazard. Mater. 153 (1–2), 164–172. https://doi.org/10.1016/j.jhazmat.2007.08.031.

Mourabet, M., El Rhilassi, A., El Boujaady, H., Bennani-Ziatni, M., El Hamri, R., Taitai, A., 2015. Removal of fluoride from aqueous solution by adsorption on hydroxyapatite (HAp) using response surface methodology. J. Saudi Chem. Soc. 19 (6), 603–615. https://doi.org/10.1016/j.jscs.2012.03.003.

Nabbou, N., Belhachemi, M., Boumelik, M., Merzougui, T., Lahcene, D., Harek, Y., Zorpas, A.A., Jeguirim, M., 2019. Removal of fluoride from groundwater using natural clay (kaolinite): Optimization of adsorption conditions. C. R. Chim. 22 (2–3), 105–112. https://doi.org/10.1016/j.crci.2018.09.010.

Oulebsir, A., Chaabane, T., Zaidi, S., Omine, K., Alonzo, V., Darchen, A., Msagati, T.A.M., Sivasankar, V., 2020. Preparation of mesoporous alumina electro-generated by electrocoagulation in NaCl electrolyte and application in fluoride removal with consistent regenerations. Arab. J. Chem. 13 (1), 271–289. https://doi.org/10.1016/j.arabjc.2017.04.007.

Pangdaeng, S., Sata, V., Aguiar, J.B., Pacheco-Torgal, F., Chindaprasirt, P., 2015. Apatite formation on calcined kaolin–white Portland cement geopolymer. Mater. Sci. Eng. C. 51, 1–6. https://doi.org/10.1016/j.msec.2015.02.039.

Pangdaeng, S., Sata, V., Chindaprasirt, P., 2018. Effect of sodium hydroxide concentration and sodium silicate to sodium hydroxide ratio on properties of calcined kaolin-white Portland cement geopolymer. Int. J. GEOMATE. 14 (46), 121–128. https://doi.org/10.21660/2018.46.mat40.

Pongener, C., Bhomick, P.C., Supong, A., Baruah, M., Sinha, U.B., Sinha, D., 2018. Adsorption of fluoride onto activated carbon synthesized from Manihot esculenta biomass—Equilibrium, kinetic and thermodynamic studies. J. Environ. Chem. Eng. 6 (2), 2382–2389. https://doi.org/10.1016/j.jece.2018.02.045.

Prasanphan, S., Wannagon, A., Kobayashi, T., Jiemsirilers, S., 2019. Reaction mechanisms of calcined kaolin processing waste-based geopolymers in the presence of low alkali activator solution. Constr. Build. Mater. 221, 409–420. https://doi.org/10.1016/j.conbuildmat.2019.06.116.

Prud'Homme, E., Michaud, P., Joussein, E., Peyratout, C., Smith, A., Rossignol, S., 2011. In situ inorganic foams prepared from various clays at low temperature. Appl. Clay Sci. 51 (1–2), 15–22. https://doi.org/10.1016/j.clay.2010.10.016.

Ren, D., Yan, C., Duan, P., Zhang, Z., Li, L., Yan, Z., 2017. Durability performances of wollastonite, tremolite and basalt fiber reinforced metakaolin geopolymer composites under sulfate and chloride attack. Constr. Build. Mater. 134, 56–66. https://doi.org/10.1016/j.conbuildmat.2016.12.103.

Rowles, M., O'connor, B., 2003. Chemical optimisation of the compressive strength of aluminosilicate geopolymers synthesised by sodium silicate activation of metakaolinite. J. Mater. Chem. 13, 1161–1165. https://doi.org/10.1039/b212629j.

Samant, A., Nayak, B., Misra, P.K., 2017. Kinetics and mechanistic interpretation of fluoride removal by nanocrystalline hydroxyapatite derived from Limacine artica shells. J. Environ. Chem. Eng. 5 (6), 5429–5438. https://doi.org/10.1016/j.jece.2017.09.058.

Sani, T., Gómez-Hortigüela, L., Perez-Pariente, J., Chebude, Y., Díaz, I., 2016. Defluoridation performance of nano-hydroxyapatite/stilbite composite compared with bone char. Sep. Purif. Technol. 157, 241–248. https://doi.org/10.1016/j.seppur.2015.11.014.

Sawangjang, B., Induvesa, P., Wongrueng, A., Pumas, C., Wattanachira, S., Rakruam, P., Punyapalakul, P., Takizawa, S., Khan, E., 2021. Evaluation of Fluoride Adsorption Mechanism and Capacity of Different Types of Bone Char. Int. J. Environ. Res. Public Health. 18 (13), 6878. https://doi.org/10.3390/ijerph18136878.

Singh, J., Singh, P., Singh, A., 2016. Fluoride ions vs removal technologies: A study. Arab. J. Chem. 9 (6), 815–824. https://doi.org/10.1016/j.arabjc.2014.06.005.

Sundaram, C.S., Viswanathan, N., Meenakshi, S., 2009. Fluoride sorption by nano-hydroxyapatite/chitin composite. J. Hazard. Mater. 172 (1), 147–151. https://doi.org/10.1016/j.jhazmat.2009.06.152.

Sutthi, N., Pranudta, A., Padungthon, S., Laonapakul, T., 2020. Synthesis of Hydroxyapatite from Bovine Bone and The Absorption of Fluoride Ions in Water. J. Ind. Tech. UBRU. 10 (2), 13–24 https://ph01.tci-thaijo.org/index.php/jitubru/article/view/185205.

Sutthi, R., Pangdaeng, S., Chindaprasirt, P., Otsuka, Y., Mutoh, Y., Laonapakul, T., 2016. Hydroxyapatite from golden apple snail shell with calcined kaolin for biomaterial applications. Key Eng. Mater. 718, 133–138. https://doi.org/10.4028/www.scientific.net/KEM.718.133.

Sutthi, R., Kaewwinud, N., Chindaprasirt, P., Mutoh, Y., Laonapakul, T., 2018. Effect of curing temperature and time on the mechanical properties of hydroxyapatite/calcined kaolin. Sci. 44 (6), 397–402. https://doi.org/10.2306/scienceasia1513-1874.2018.44.397.

Swain, S.K., Mishra, S., Sharma, P., Patnaik, T., Singh, V.K., Jha, U., Patel, R.K., Dey, R.K., 2010. Development of a New Inorganic-Organic Hybrid Ion-Exchanger of Zirconium(IV)-Propanolamine for Efficient Removal of Fluoride from Drinking Water. Ind. Eng. Chem. Res. 49, 9846–9856. https://doi.org/10.1021/ie1012536.

Tahaikt, M., Ait Haddou, A., El Habbani, R., Amor, Z., Elhannouni, F., Taky, M., Kharif, M., Boughriba, A., Hafsi, M., Elmidaoui, A., 2008. Comparison of the performances of three commercial membranes in fluoride removal by nanofiltration. Continuous operations. Desalination. 225 (1–3), 209–219. https://doi.org/10.1016/j.desal.2007.07.007.

Tan, I.A.W., Ahmad, A.L., Hameed, B.H., 2008. Adsorption of basic dye on high-surface-area activated carbon prepared from coconut husk: Equilibrium, kinetic and thermodynamic studies. J. Hazard. Mat. 154 (1–3), 337–346. https://doi.org/10.1016/j.jhazmat.2007.10.031.

Uddin, M.K., Ahmed, S.S., Naushad, M., 2019. A mini update on fluoride adsorption from aqueous medium using clay materials. Desalination Water Treat. 145, 232–248. https://doi.org/10.5004/dwt.2019.23509.

Veloso, C.H., Filippov, L.O., Filippova, I.V., Ouvrard, S., Araujo, A. C., 2020. Adsorption of polymers onto iron oxides: Equilibrium isotherms. J. Mater. Res. Technol. 9 (1), 779–788. https://doi.org/10.1016/j.jmrt.2019.11.018.

Wang, Y., Chen, N., Wei, W., Cui, J., Wei, Z., 2011. Enhanced adsorption of fluoride from aqueous solution onto nanosized hydroxyapatite by low-molecular-weight organic acids. Desalination 276 (1–3), 161–168. https://doi.org/10.1016/j.desal.2011.03.033.

Xiong, X.Z., Lui, J.L., He, W.H., Xia, T., He, P., Chen, X.M., Yang, K.D., Wang, A.G., 2007. Dose-effect relationship between drinking water fluoride levels and damage to liver and kidney functions in children. Environ. Res. 103 (1), 112–116. https://doi.org/10.1016/j.envres.2006.05.008.

Xu, X., Li, Q., Cui, H., Pang, J., Sun, L., An, H., Zhai, J., 2011. Adsorption of fluoride from aqueous solution on magnesia-loaded fly ash cenospheres. Desalination 272 (1–3), 233–239. https://doi.org/10.1016/j.desal.2011.01.028.

Zhang, Y., Wang, D., Liu, B., Gao, X., Xu, W., Liang, P., Xu, Y., 2013. Adsorption of Fluoride from Aqueous Solution Using Low-Cost Bentonite/Chitosan Beads. Am. J. Anal. Chem. 4, 48–53. https://doi.org/10.4236/ajac.2013.47A007.

Zhao, X., Li, Y., Carroll, K.C., Li, F., Qiu, L., Huo, Z., 2021. Mesoporous goethite for rapid and high-capacity fluoride removal from drinking water. J. Environ. Chem. Eng. 9, (4). https://doi.org/10.1016/j.jece.2021.105278 105278.

Zúñiga-Muro, N.M., Bonilla-Petriciolet, A., Mendoza-Castillo, D.I., Reynel-Ávila, H.E., Tapia-Picazoa, J.C., 2017. Fluoride adsorption properties of cerium-containing bone char. J. Fluor. Chem. 197, 63–73. https://doi.org/10.1016/j.jfluchem.2017.03.004.